Electronic Supplementary Material (ESI) for RSC Advances.
This journal is © The Royal Society of Chemistry 2016

High-performance carbon-coated mesoporous $LiMn_2O_4$ cathode materials synthesized from a novel hydrated layered-spinel lithium manganate composite

Caihua Jiang[1], Zilong Tang*[1], Shiqing Deng[1,2], Ye Hong[1], Shitong Wang[1] and Zhongtai Zhang[1]

[1]*State Key Laboratory of New Ceramics and Fine Processing, School of Materials Science and Engineering, Tsinghua University, Beijing 100084, P.R. China*

[2]*National Center for Electron Microscopy in Beijing, School of Materials Science and Engineering, The State Key laboratory of New Ceramics and Fine Processing, Key Laboratory of Advanced Materials (MOE), Tsinghua University, Beijing 100084, P.R. China*

**corresponding author*

Tel: +86 10 62783685; Fax: +86 10 62771160

E-mail address: tzl@tsinghua.edu.cn

Contents:

Experimental Details

Synthesis of the hydrated layered-spinel lithium manganate composite (Hydrated L-S).

First of all, the manganese oxide (denoted as MO) was prepared as hydrothermal precursor based on a redox reaction of $HMnO_4$ [S1] with slight modifications. Briefly, 0.03 M homogeneous $KMnO_4$ solution was injected by 0.5 mL H_2SO_4 (2.5 M) and stirred for 0.5 h. Subsequently, 3 mL absolute ethanol was dropped into the above solution. After another 3 h redox reaction, the black brown suspension was vacuum-filtered and washed with deionized water for three times. Next, the as-prepared MO was added into a certain concentration of LiOH solution under magnetic stirring followed by the transfer into a 50 mL Teflon-lined stainless steel autoclave. The autoclave was kept at 160 ℃ for 48 h in an oven and then cooled down to room temperature naturally. Finally, the hydrothermal precipitate was vacuum-filtered, washed with deionized water and dried at 70 ℃ overnight under vacuum, thus obtaining the hydrated lithium manganate composite (Hydrated L-S).

Synthesis of the carbon-coated mesoporous spinel $LiMn_2O_4$ (LMO-CM).

The as-obtained hydrothermal product of the hydrated layered-spinel lithium manganate composite was annealed at 600 ℃ for 6 h with a heating rate of 3 ℃ min^{-1} under vacuum. Thus, the carbon-coated mesoporous spinel $LiMn_2O_4$ (denoted as LMO-CM) was synthesized. Meanwhile, in order to synthetically compare the electrochemical performances, two control groups were introduced: the no carbon-coated spinel $LiMn_2O_4$ (denoted as LMO-NC) which was annealed in air with the other

experimental variables the same as those of LMO-CM and the commercial spinel lithium manganese oxide (denoted as LMO-COM).

Detailed descriptions of the synthetic process for preparing surface carbon layer.

The synthetic process used for preparing surface carbon layer can be briefly divided into three steps [S1]:

(I) Reduction reaction between $HMnO_4^-$ and CH_3CH_2OH under acid conditions.

$$2KMnO_4 + H_2SO_4 = 2HMnO_4 + K_2SO_4$$

$$HMnO4 + CH_3CH_2OH \rightarrow MnO_2 + CH_3CO_2H + H_2O$$

After the reaction, the MnO_2 nanosheets can be stabilized by the CH_3COO^- group and the organic group can remain absorbed on the surface of the nanosheets.

(II) Hydrothermal process using the obtained CH_3COO^- group adsorbed MnO_2 nanosheets in LiOH aqueous solution.

During the reaction, new MnO_2 nuclei adsorbed with the CH_3COO^- group might be formed and a novel mesoporous hydrated layered-spinel lithium manganate composite was obtained.

(III) Heat treatment under vacuum to obtain $LiMn_2O_4$ terminated with amorphous carbon.

Through the annealing treatment, the carbon layer can be generated attributed to the carbonization of absorbed organic groups.

Characterization of materials

The crystallographic structures were characterized by powder X-ray diffraction (XRD, Cu Kα, D8 ADVANCE A25, Bruker, Germany) at $6\,^\circ\,min^{-1}$. Morphology structure, crystallographic characteristics and surface feature were obtained by field-emission scanning electron microscopy (SEM, MERLIN VP Compact, ZEISS, Germany), transmission electron microscopy (TEM, HT7700, Hitachi, Japan) and high resolution transmission electron microscopy (HRTEM, JEOL-2100, JEOL, Japan)

equipped with energy dispersive spectrometer (EDS). EDS point mapping was conducted on the JEM 2010F TEM with an X-Max 80 Instrument detector in bright scanning transmission electron microscopy (STEM) mode. X-ray photoelectron spectroscopy (XPS) was carried out on an ESCALAB 250Xi instrument (Thermo Fisher Scientific, USA). Inductively coupled plasma optical emission spectrometry (ICP-OES) was measured on a Thermo Fisher Scientific tester (iCAP6300, USA). Thermogravimetric-differential thermal analysis (TG-DTA) was performed using a STA 449 F3 thermogravimetric analyzer (NETZSCH, Germany) from ambient temperature to 600 ℃ with a heating rate of 10 ℃ min^{-1} under nitrogen atmosphere. Nitrogen adsorption-desorption experiments and pore structure analysis were carried out by an Autosorb-iQ2-MP surface area and porosimetry analyzer (Quantachrome, USA) at 77.4 K. Pore-size distributions were calculated by density functional theory (DFT) method. The carbon content was measured by a EuroEA3000 elemental analyzer (Euro Vector S.P.A., Italy).

Electrochemical measurements

Active materials (e.g. LMO-CM), conductive carbon black (Super P), and polymer binder (polyvinylidene fluoride, PVDF) were homogenously mixed with a weight ratio of 70: 20: 10 in an N-methyl-2- pyrrolidene (NMP) solvent. The obtained viscous slurry was then pasted on aluminum foils and dried in a vacuum oven at 110 ℃ overnight. Then, the film was pressed and punched into discs as working electrodes and the mass loading of the active material was controlled between 0.8-1.2 mg cm^{-2}. The electrochemical performances were evaluated by assembling CR2032 coin type cells

wherein pure lithium discs were used as both counter and reference electrodes, 1 mol L^{-1} $LiPF_6$ in carbonate (EC)/ dimethyl carbonate (DMC)/ ethyl methyl carbonate (EMC) (1: 1: 1 by volume) was used as electrolyte and microporous membrane (Celgard 2400, Japan) was used as separator. The whole assembly process was performed in an argon-filled glove box.

The galvanostatic discharge/charge tests were conducted on a LAND Cell test 2001 A system (Wuhan, China). For the rate performance tests and cycling performance tests at 0.2 C (1 C =140 mA g^{-1}), the cell was charged at the required rate to 4.3 V, and held at 4.3 V until the current density decreased to 10 % of the initial value, and then discharged to 3.2 V at the same rate as charging. While for the other cycling tests at higher current density such as 30 C, 60 C, 80 C and 120 C, the activation process was employed which can help form a stable SEI film and ensure better performances. During the first two cycles, cells were charged in segmented potential ranges and then discharged at a very low current density. From the third cycle, the test procedure remained the same as the abovementioned operations for rate performance tests. Herein, for these measurements, we regard capacity in the third cycle as the initial value and capacity in the 1502nd cycle as the value of the 1500th cycle throughout the whole article for explanations and comparisons. Zahner IM6 electrochemical workstation was used for cyclic voltammetry (CV) and electrochemical impedance spectra (EIS) measurements. CV measurements was tested at a sweep rate of 0.1 mV s^{-1} between 3.1 V and 4.4 V and EIS measurements were tested in the completely discharged state after 50 cycles at 30 C at the frequency ranging from 0.01 Hz to 100 kHz. All the

electrochemical tests were carried out at room temperature.

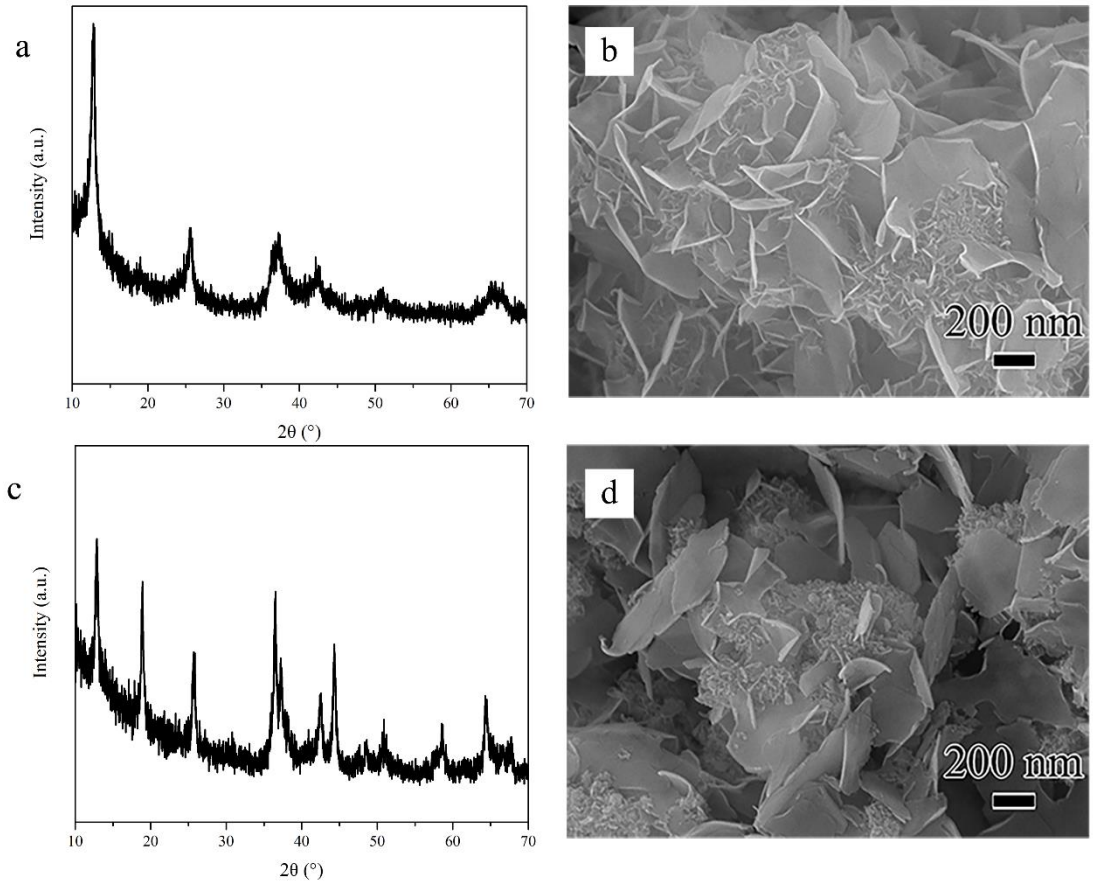

Fig. S1 Phase characterization and morphology of hydrothermal products at intermediate time. (a, c) XRD patterns and (b, d) SEM image of the hydrothermal products after 1 h and 3 h reaction, respectively.

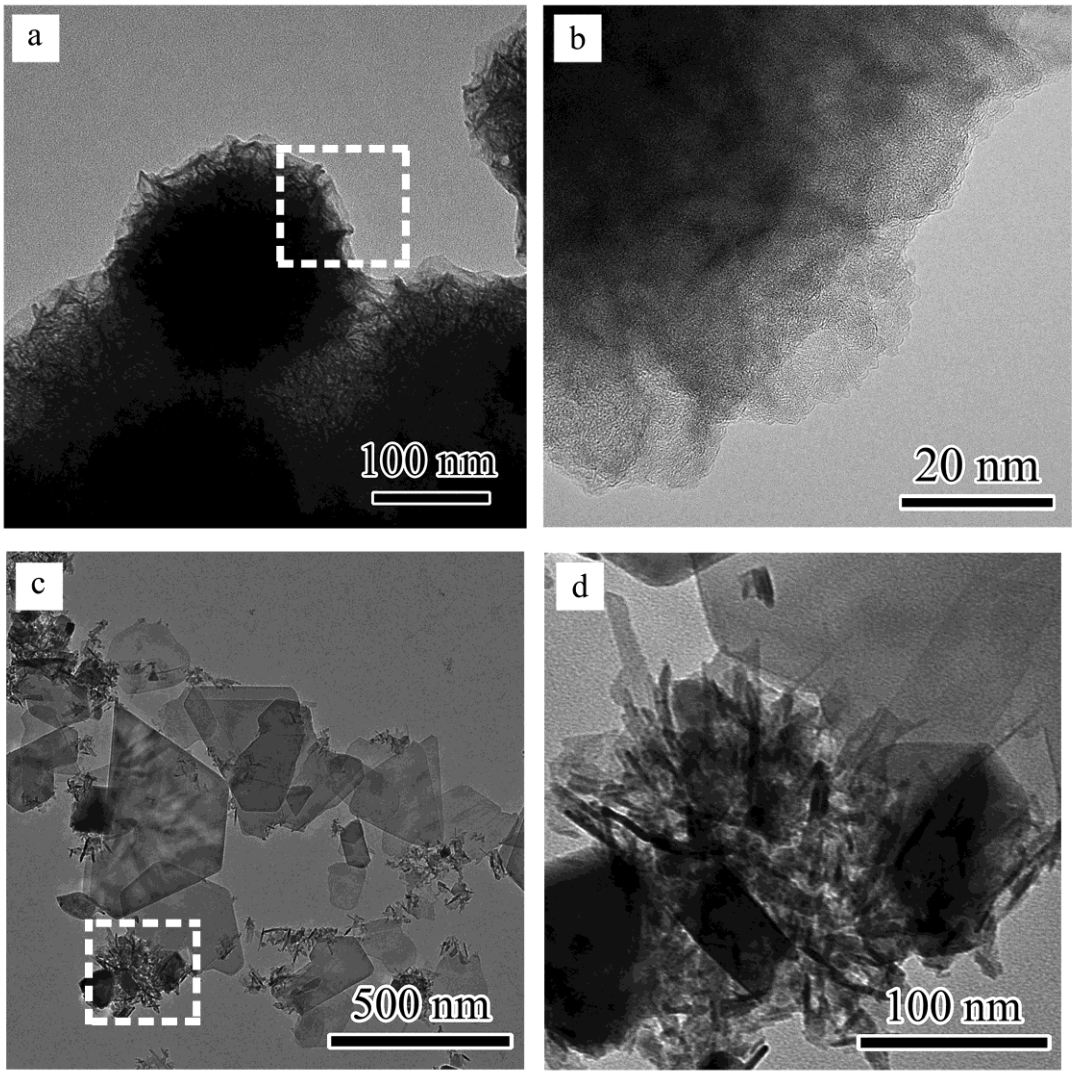

Fig. S2 (a-b) TEM images of the initial manganese oxide MO. (c-d) TEM images of the hydrated layered-spinel lithium manganese oxide composite (Hydrated L-S). Fig. S2b and Fig. S2d are the enlarged view of the dotted area in (a) and (c), respectively.

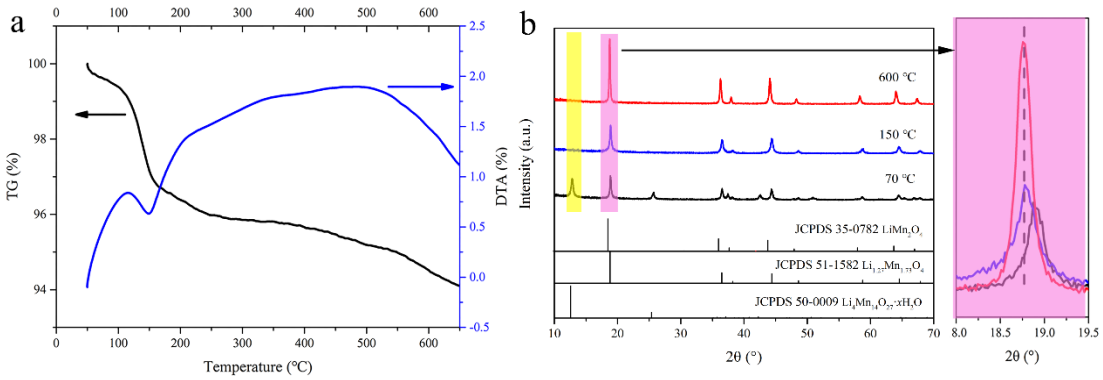

Fig. S3 (a) TG-DTA curves of the Hydrated L-S. (b) Comparison of XRD patterns for

samples annealed at different temperature.

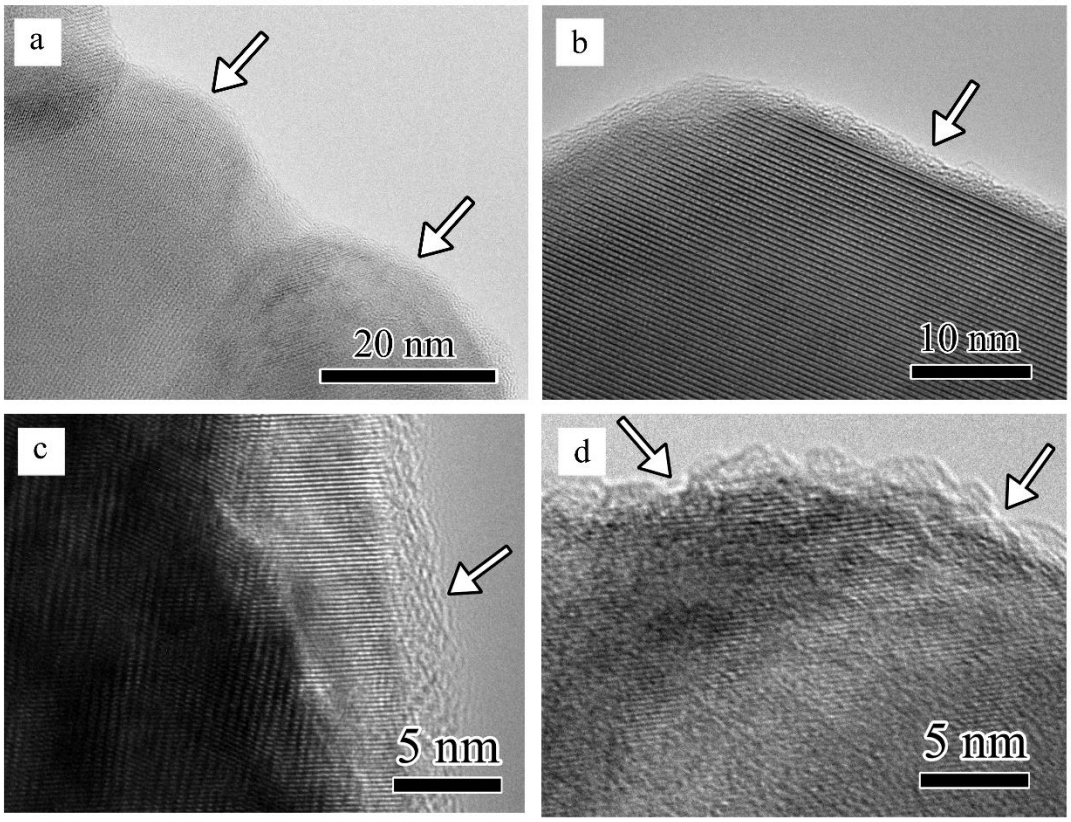

Fig. S4 HRTEM images of LMO-CM showing the continuous carbon layer.

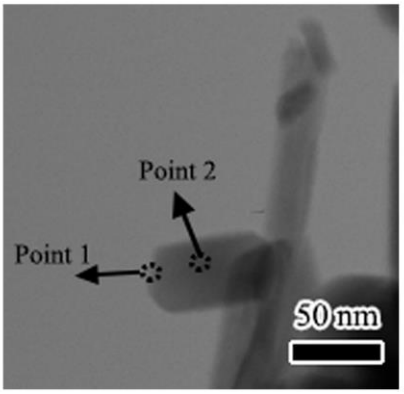

Point 1		
Element	Weight(%)	Atomic(%)
C	5.6	11.34
O	43.5	66.13
Mn	50.9	22.53
Total	100	100

Point 2		
Element	Weight(%)	Atomic(%)
C	1.43	2.78
O	53.42	78.02
Mn	45.15	19.2
Total	100	100

Fig. S5 EDS point mapping analysis of C, O and Mn relative concentrations at the edge and middle zone of the as-prepared spinel $LiMn_2O_4$.

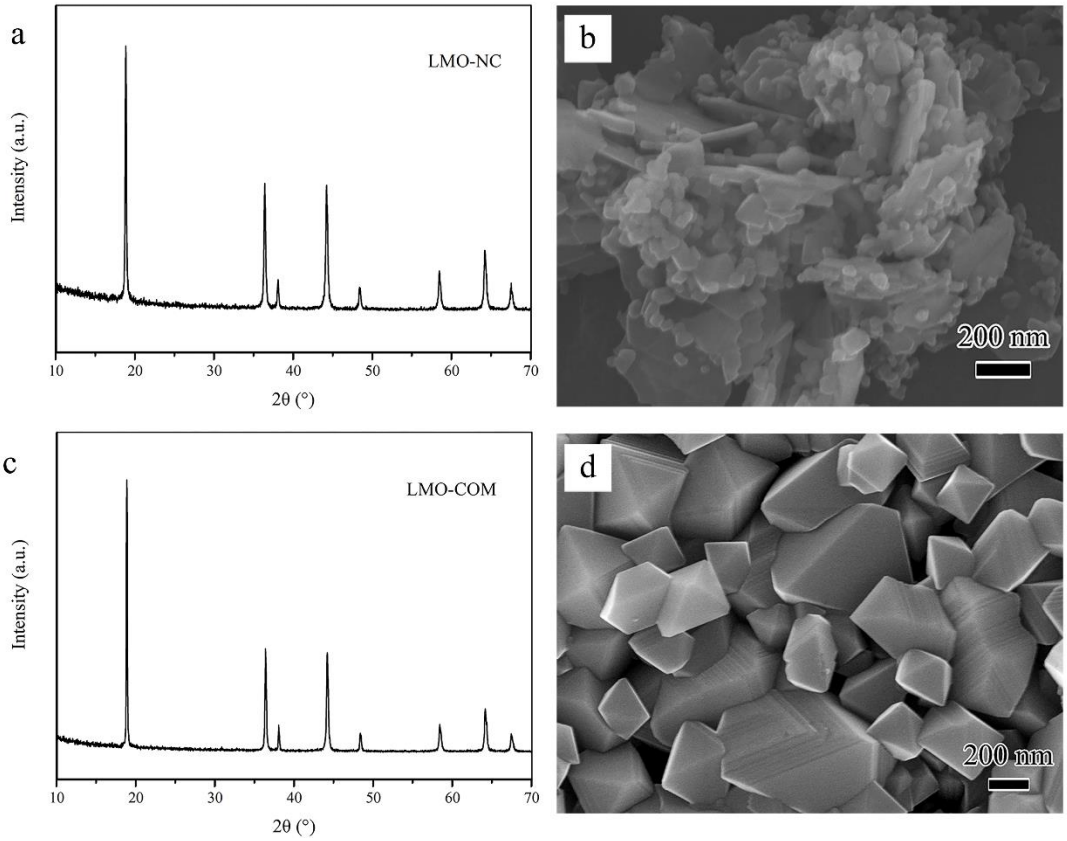

Fig. S6 (a, c) Typical XRD patterns and (b, d) SEM images of the no carbon-coated LMO-NC and the commercial LMO-COM, respectively. LMO-NC processes the similar morphology as LMO-CM and LMO-COM retains the polyhedral shape of uneven sizes. Both of the two samples can be indexed to pure spinel $LiMn_2O_4$ without impurity.

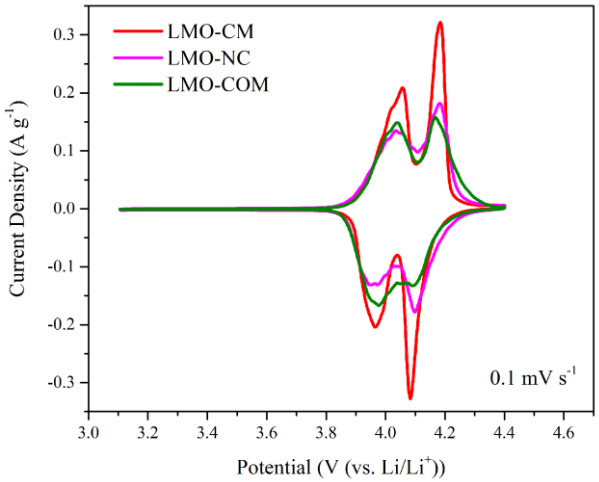

Fig. S7 Cyclic voltammograms at the scanning rate of 0.1 mV s^{-1} with a cut-off voltage

window of 3.1–4.4 V vs. Li/Li^+ for the carbon-coated LMO-CM, no carbon-coated LMO-NC and the commercial LMO-COM.

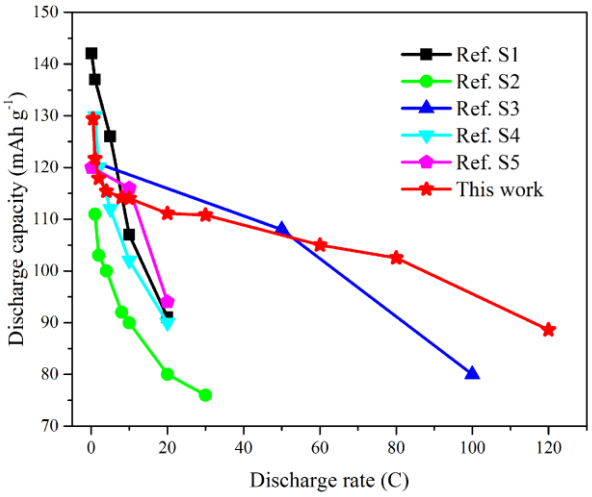

Fig. S8 Rate capability comparison between typical high-rate LMO/C materials (carbon-coated $LiMn_2O_4$ nanowires [S1], carbon-encapsulated $LiMn_2O_4$ spheres [S2], carbon-coated $LiMn_2O_4$ nanoparticle clusters [S3], sea cucumber-like $LiMn_2O_4$/C composite [S4], $LiMn_2O_4$/MWCNTs nanocomposite [S5]) and our work.

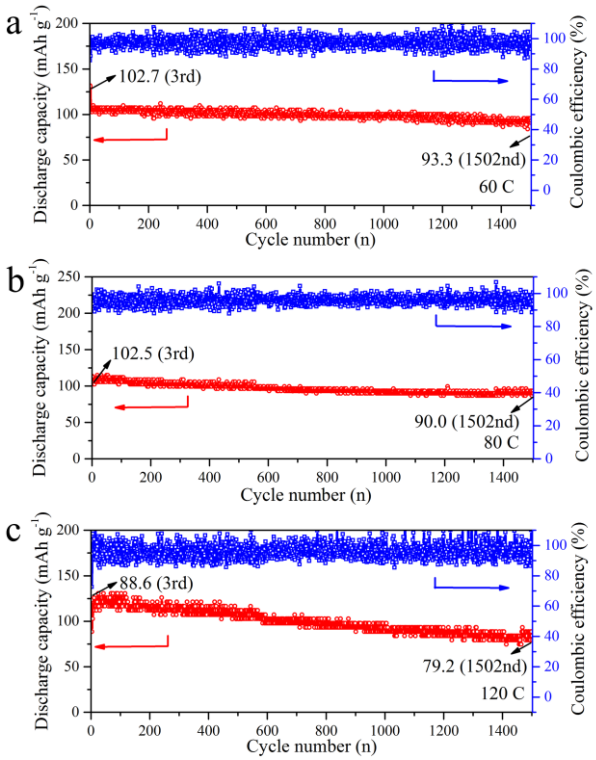

Fig. S9 Cycling performance at high rates of 60 C (a), 80 C (b) and 120 C (c) for LMO-CM.

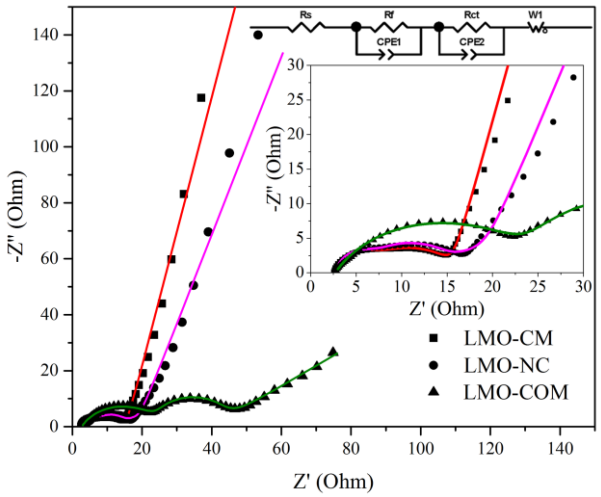

Fig. S10 Electrochemical impedance spectrum (EIS) of LMO-CM, LMO-NC and LMO-COM after 50 cycles at 30 C where the tested impedance data are in good agreement with the fitting results using the inset equivalent circuit. R_s: the resistance of the electrolytes; R_f: Li^+ migration through the surface film; CPE1: surface film capacitance; R_{ct}: charge transfer resistance; CPE2: double-layer capacitance and Z_w: Warburg resistance.

References

S1. W. Sun, H. Liu, Y. Liu, G. Bai, W. Liu, S. Guo and X. Z. Zhao, *Nanoscale*, 2015, **7**, 13173-13180.

S2. H. Zhang, Z. Li, S. Yu, Q. Xiao, G. Lei and Y. Ding, *J. Power Sources*, 2016, **301**, 376-385.

S3. S. Lee, Y. Cho, H.-K Song, K. T. Lee and J. Cho, *Angew. Chem., Int. Ed*, 2012, **51**, 8748-8752.

S4. J. Wang, W. Liu, S. Liu, J. Chen, H. Wang and S. Zhao, *Electrochim. Acta*, 2016,

188, 645-652.

S5. F. v. Bülow, H. Zhang, D. E. Morse, *Adv. Energy Mater.*, 2012, **2**, 309-315.